Assessment of the Impacts of Different Carbon Sources and Sinks on Atmospheric CO2 Concentrations Based on the GEOS-Chem Model

Ge Qu , Jia Zhou * , Yusheng Shi * , Yong liang Yang , Meng qian Su , Wen Wu , Zhi tao Zhou

Posted Date: 31 January 2025

doi: 10.20944/preprints202501.2368.v1

Keywords: CO2 concentrations; GEOS-Chem model; Inventory switching and replacing; Model simulations; Spatiotemporal characteristics

Article

Assessment of the Impacts of Different Carbon Sources and Sinks on Atmospheric CO_2 Concentrations Based on the GEOS-Chem Model

Ge Qu [1,2], Jia Zhou [1,*], Yusheng Shi [2,*], Yongliang Yang [3], Mengqian Su [3], Wen Wu [1] and Zhitao Zhou [3]

[1] Heilongjiang Province Key Laboratory of Geographical Environment Monitoring and Spatial Information Service in Cold Regions, Harbin Normal University, Harbin 150025, China; quge@hrbnu.edu.cn

[2] State Key Laboratory of Remote Sensing Science, Aerospace Information Research Institute, Chinese Academy of Sciences, Beijing 100101, China

[3] College of Resources and Environment, University of Chinese Academy of Sciences, Beijing 101408, China

* Correspondence: harbin_zhoujia@hrbnu.edu.cn; Tel.: +86-10-6485-2835

Abstract: Global CO_2 concentration has become a key driver of climate change, influenced by both anthropogenic emissions and natural carbon cycles. However, due to the spatiotemporal heterogeneity of carbon sources and sinks, estimating CO_2 flux remains highly uncertain. Accurately quantifying the contribution of various carbon sources and sinks to atmospheric CO_2 concentration is essential for understanding the carbon cycle and global carbon balance. This study utilizes the GEOS-Chem model, driven by MERRA2 meteorological data and emission inventory data, to simulate monthly global CO_2 concentrations from 2006 to 2010. The "Inventory switching and replacing" method was applied to assess the contributions of eight major CO_2 sources and sinks: fossil fuel combustion, biomass burning, biosphere balance, net land exchange, aviation, shipping, ocean exchange, and chemical sources. The results show that global CO_2 concentration exhibits a spatial pattern with higher concentrations in the Northern Hemisphere and land areas, with East Asia, Southeast Asia, and Eastern North America being high-concentration regions. The global average CO_2 concentration increased by 1.8 ppm/year from 2006 to 2010, with China's eastern region experiencing the highest growth rate of 3.0 ppm/year. Fossil fuel combustion is identified as the largest CO_2 emission source, followed by biomass burning, while oceans and land serve as significant CO_2 sinks. The impact of carbon flux on atmospheric CO_2 concentration is closely related to the spatial distribution and magnitude of emissions.

Keywords: CO_2 concentrations; GEOS-Chem model; Inventory switching and replacing; Model simulations; Spatiotemporal characteristics

1. Introduction

Global warming has become one of the most pressing environmental challenges facing the world today. The dramatic increase in atmospheric carbon dioxide (CO_2) concentration is widely considered one of the primary drivers of climate change. According to the Annual Greenhouse Gas Index (AGGI) report from the National Oceanic and Atmospheric Administration (NOAA), the total radiative forcing of global greenhouse gases increased by 49% from 1990 to 2023, with CO_2 accounting for approximately 80% of this increase. In 2023, the global annual average CO_2 concentration reached 419.3 ± 0.1 ppm, representing a 51% increase relative to pre-industrial levels (NOAA GML). Furthermore, the annual CO_2 growth rate in 2023 was 2.8 ± 0.01 ppm·year^{-1}, a slight increase compared to the previous year [1]. The continued rise in CO_2 concentration has exacerbated global warming and placed immense pressure on the global climate system, making it a central driving force of climate change.

 doi:10.20944/preprints202501.2368.v1

Changes in atmospheric CO_2 concentration are influenced not only by anthropogenic carbon emissions but also by natural carbon cycles. The global carbon budget is a key regulatory factor in the variability of atmospheric CO_2 concentration, with carbon sources (such as fossil fuel combustion and biomass burning) and carbon sinks (such as terrestrial and oceanic carbon absorption) jointly controlling CO_2 emissions and absorption [1]. However, due to the spatial distribution, temporal variability, and assessment methods of both carbon sources and sinks, there is considerable uncertainty in CO_2 flux estimates, which presents a significant challenge for accurately predicting atmospheric CO_2 concentrations [2,3]. Carbon sources and sinks exhibit significant spatiotemporal heterogeneity, with their emissions characterized by randomness, seasonality, broad distribution, and difficulties in monitoring. Understanding the precise spatiotemporal variations of these carbon sources and sinks and quantifying their impacts on atmospheric CO_2 concentration is of great scientific importance and practical value for addressing climate change and formulating effective carbon emission control policies.

To study the spatiotemporal changes in atmospheric CO_2 concentration, scientists widely use atmospheric chemical transport models. These models simulate the variations in meteorological data and source-sink fluxes, effectively reflecting the dynamic characteristics of CO_2 concentration in the atmosphere [4]. Validation of these models using ground-based, airborne, and satellite observations is one of the commonly used methods. For instance, Feng et al. (2011) [5] combined ground and satellite observational data from 2003 to 2006 to assess the performance of the global chemical transport model GEOS-Chem in simulating CO_2 concentrations. The GEOS-Chem model has demonstrated excellent performance in CO_2 inversion and estimating surface carbon fluxes (https://geos-chem.seas.harvard.edu/). For example, Zeng et al. (2022) [6] utilized GEOS-Chem to investigate the global and regional impacts of changes in the biosphere and climate anomalies on atmospheric CO_2 concentrations.

In chemical transport models, the variation in CO_2 concentration is driven by various carbon sources and sinks and is regulated by atmospheric transport processes. Existing studies show that emission sources, such as fossil fuel combustion, biomass burning, and biofuel use, contribute significantly to CO_2 concentration, with considerable spatial variability in their emissions [7]. On the carbon sink side, the absorption of CO_2 by terrestrial ecosystems and oceans plays a crucial role in regulating atmospheric CO_2 levels. Through simulation analysis, researchers have found that fossil fuel combustion is the largest global CO_2 emission source, while the flux variations in the biosphere are the main cause of seasonal fluctuations in atmospheric CO_2 concentrations. Nassar et al. (2010) [8] demonstrated that aviation and maritime emissions significantly increase the latitudinal gradient of global CO_2 concentrations, whereas the impact of chemical sources is relatively minor. Furthermore, oceanic and terrestrial carbon exchanges play a significant role in mitigating the rise in atmospheric CO_2 concentrations [9].

Although numerous studies have explored the role of individual carbon sources or sinks, most have focused on the effects of major carbon sources and sinks such as fossil fuel combustion and terrestrial carbon fluxes, with relatively few addressing the combined effects of different carbon sources and sinks on atmospheric CO_2 concentrations and their interrelationships [1]. This study, based on the GEOS-Chem atmospheric chemical transport model, simulates the global atmospheric CO_2 concentrations from 2006 to 2010, analyzes the spatial distribution and temporal variations of CO_2 concentrations, and validates the model using NOAA-ESRL ground-based observation data and GOSAT satellite data to assess its accuracy. Additionally, through a series of numerical experiments, this study investigates the impacts of eight major CO_2 sources and sinks (fossil fuel combustion, biomass burning, biospheric equilibrium, net land exchange, maritime, aviation, oceanic exchange, and chemical sources) on global atmospheric CO_2 concentration variations. By comparing the results, this study reveals the contribution differences of various CO_2 sources and sinks to atmospheric CO_2 concentration changes in different regions of the world. This research will provide new insights into understanding the mechanisms of atmospheric CO_2 variation in the global carbon cycle and offer scientific support for the accurate validation of global carbon emission inventories and the formulation of climate policies.

 doi:10.20944/preprints202501.2368.v1

2. Date and Methods

2.1. GEOS-Chem Model Description

The continuously improving 3-D atmospheric chemical transport model GEOS-Chem describes atmospheric transmission, diffusion, reaction, and elimination on local to global scales. The GEOS-Chem CO_2 simulation capability was first developed by Suntharalingam et al (2003, 2004) [7,10] and updated by Nassar et al (2010) [11]. Here, we used GEOS-Chem Classic version 13.2.1 (http://www.geos-chem.org/) for the global CO_2 concentration simulations. The model grid was selected with a horizontal resolution of 2.5° longitude × 2.0° latitude and 47 vertical hybrid-sigma layers up to 0.01 hPa. The simulations were driven by the Modern-Era Retrospective Analysis for Research and Applications, Version 2 (MERRA-2) meteorological fields from the Goddard Earth Observing System (GEOS) of the NASA Global Modeling and Assimilation Office (GMAO) [12]. CO_2 was transported as a tracer in the model with prescribed prior CO_2 fluxes. These included biomasses burning emission, fossil fuel emission, ocean exchange emission, balanced biosphere exchange, net terrestrial exchange, ship emission, aviation emission, and CO_2 chemical sources from the oxidation of atmospheric carbon species such as carbon monoxide (CO), methane (CH_2), and non-methane volatile organic compounds (NMVOCs) (Table 1).

Table 1. List of CO_2 emission inventories used in the GEOS-Chem simulations in this study.

Flux Type	Inventory Name Abbreviation	Description	Spatial	Temporal	References
Biomass Burning	QFED	Quick Fire Emissions Database for 2006-2010	0.1° × 0.1°	Daily	[13]
Fossil Fuel	ODIAC	Open source Data Inventory for Atmospheric CO_2 for 2006-2010	1° × 1°	Monthly	[14]
Ocean Exchange	Scaled ocean exchange	Scaled ocean exchange for 2006-2010	4° × 5°	Monthly	[15]
Balanced Biosphere	SIB3	Balanced Net Ecosystem Production (NEP) CO_2 for 2006-2010	1° × 1.25°	3-hourly	[16]
Net Terrestrial Exchange	TransCom climatology	TransCom net terrestrial biospheric CO_2 fixed in 2000	1° × 1°	Fixed	[17]
Ship	CEDS	Community Emissions Data System for 2006-2010	0.5° × 0.5°	Monthly	[18]
Aviation	AEIC	Aircraft Emissions Inventory Code fixed in 2005	1°×1°	Monthly	[19]
Chemical Source	CO_2 Chemical Source	CO_2 chemical production from carbon species oxidation fixed in 2004	2°×2.5°	Monthly	[20]

2.2. Numerical Experiments

A uniform initial global average CO_2 concentration value of 373.71 ppm was set for January 1, 2003, based on the annual mean marine surface CO_2 concentration from the Mauna Loa Observatory in Hawaii, provided by the NOAA Earth System Research Laboratory (ESRL) [20,21]. A 3-year spin-up simulation was conducted to allow the model to reach a reasonable spatial distribution of the initial CO_2 concentration for subsequent simulations. Next, experiments were designed using the "list switch" method [22–24] to explore the effects of different emission sources on simulated atmospheric CO_2 concentration.

Simulation test: The simulation conducted with all sources enabled is called the BASE simulation. Simulations conducted with a specific emission source inventory X disabled are called

 doi:10.20944/preprints202501.2368.v1

the "no_X" simulations (where X represents FF, BB, BalB, NTE, S, A, O, and CS, respectively). The difference between the CO_2 concentration simulated by the BASE and the CO_2 concentration simulated by the no_X setup represents the influence of emission source X on the simulated atmospheric CO_2 concentration. The experimental design is shown in Table 2.

Table 2. Simeulation test.

Flux Type	Inventory Name Abbreviation	Experiments [1]								
		BASE	no_FF	no_BB	no_BalB	no_NTE	no_S	no_A	no_O	no_CS
Fossil Fuel	FF	+	–	+	+	+	+	+	+	+
Biomass Burning	BB	+	+	–	+	+	+	+	+	+
Balanced Biosphere	BalB	+	+	+	–	+	+	+	+	+
Net Terrestrial Exchange	NTE	+	+	+	+	–	+	+	+	+
Ship	S	+	+	+	+	+	–	+	+	+
Aviation	A	+	+	+	+	+	+	–	+	+
Ocean Exchange	O	+	+	+	+	+	+	+	–	+
Chemical Source	CS	+	+	+	+	+	+	+	+	–

[1] "+" indicates that the emission list is enabled, and "-" indicates that the emission list is disabled.

2.3. Model Evaluation

2.3.1. GOSAT Total Column CO_2 (XCO_2) Observations

GOSAT is equipped with a sun-synchronous orbit, with local solar time ranging from 12:45 to 13:15, a 98.1-minute orbital period, and a 10.5 km diameter circular footprint since its launch on July 1, 2009. The primary scientific instrument aboard GOSAT is the Thermal and Near Infrared Sensor for carbon Observations - Fourier Transform Spectrometer (TANSO-FTS). The Short Wave InfraRed (SWIR) detector measures the spectrum reflected from both land and water surfaces in two CO_2 spectral regions: 1.56–1.72 μm for weak CO_2 absorption and 1.92–2.08 μm for strong CO_2 absorption [25].

The Total Carbon Column Observing Network (TCCON) provides high-precision XCO_2 data products and serves as a crucial validation resource for GOSAT [26]. GOSAT XCO_2 measurements have shown good agreement with TCCON data globally [27,28]and exhibit strong seasonal consistency with ground-based datasets after improvements to the retrieval algorithms [29,30].

In this study, we compared the BASE simulation results with the XCO_2 data retrieved from the GOSAT ACOS Level 2 Lite Data Product (full physics retrieval Version 7.3, ACOS_L2_Lite_FP.7.3). Before comparing the model outputs with GOSAT data, we performed data screening to ensure quality control. We selected a comparison area between latitudes 80°S and 80°N, excluding poor-quality soundings based on the xCO_2_quality_flag. This flag, of byte type, assigns a value of 0 for good soundings and 1 for bad soundings. To compare the simulated CO_2 concentrations from the 47 vertical levels of the model with the GOSAT XCO_2, we calculated the model's XCO_2 using the following equation [31]:

$$X_{CO2} = X_{CO2}^{a} + h^{T}A(x - x_a) = X_{CO2}^{a} + \sum_{j} h_j a_{CO2,j}(x - x_a)_j \quad (1)$$

where X_{CO2}^{a} denotes the a priori value of XCO_2, h_j is the pressure weighting function for each level, j is the atmospheric level, $a_{CO2,j}$ is the XCO_2 column averaging kernel, and x_a is the prior CO_2 profile. The above parameters were obtained from GOSAT products. A represents the full averaging kernel matrix, and x denotes the CO_2 profile calculated from the model results. The GOSAT-retrieved XCO_2 and other variables used in this study can be downloaded from the Goddard Earth Sciences Data and Information Services Center (GES DISC) archive at https://disc.gsfc.nasa.gov/.

The specific conversion process from simulated CO_2 concentration to simulated XCO_2 concentration includes:

 doi:10.20944/preprints202501.2368.v1

- Screening the a priori values to exclude abnormal or missing data.
- Re-matching the valid a priori values with the atmospheric pressure.
- Interpolating horizontally to obtain simulated data that matches the longitude and latitude of the GOSAT data.
- Interpolating vertically to obtain simulated data that matches the layers of the GOSAT data.
- Using the processed simulated data from the above steps in equation (1) to compute the simulated XCO_2.

2.3.2. Surface CO_2 Observations

The ground-based CO_2 observational data used in this study were provided by the Observation Package (ObsPack) data products from the Carbon Cycle and Greenhouse Gases (CCGG) Global Greenhouse Gas Reference Network measurement program. This program integrates direct atmospheric greenhouse gas measurements from national and university laboratories, packaging them into a set of self-documented files for distribution [32]. Continuous CO_2 measurements were conducted either in situ or through flask air sampling. These data products are maintained by NOAA ESRL (https://gml.noaa.gov/ccgg/obspack/) and are also available through the World Meteorological Organization's World Data Center for Greenhouse Gases (https://gaw.kishou.go.jp/). The reliability of the surface CO_2 observations has been validated in regions such as Asia [33], Europe [34], and globally [35,36].

Surface CO_2 observational data were sourced from the Global Greenhouse Gas Reference Network (GGGRN) and its ObsPack data product (Supplementary Information (SI) Table S1). These data, comprising monthly CO_2 measurements from January 2006 to December 2010, were collected at 30 ground-based monitoring stations distributed globally. The stations are strategically located to ensure representative spatial coverage across diverse regions. The surface CO_2 data were then used to validate the simulation results generated by the GEOS-Chem model.

The simulated CO_2 concentration was processed as follows:

- Horizontal interpolation was applied to match the latitude and longitude of the observation sites with the simulated data.
- Vertical interpolation was performed to match the elevation of the observation sites with the simulated data.

3. Results and Discussions

3.1. Simulation Verification Results

To assess the accuracy of the GEOS-Chem simulation results, we compared the simulated CO_2 concentrations with the CO_2 concentrations observed by the GOSAT satellite and NOAA-ESRL.

3.1.1. Verification Results of Satellite Observations

Using the column concentration conversion method outlined in Section 2.3.1, the simulated global stratified CO_2 concentrations were first converted into global column concentrations (XCO_2). These simulated XCO_2 values were then interpolated to the locations corresponding to the GOSAT observation points. The deviation between the simulated and GOSAT-observed XCO_2 is calculated by subtracting the GOSAT XCO_2 from the simulated XCO_2. The GOSAT satellite's effective observation samples cover nearly all continental regions of the world and oceanic areas between 45°S and 45°N, providing wide spatial coverage and making the dataset globally representative. In total, more than 86% of the sample deviations are below 3 ppm. Among these, 30.7% are between -3 and -2 ppm, 39.7% are between -2 and -1 ppm, and 12.5% are between -1 and 0 ppm.

 doi:10.20944/preprints202501.2368.v1

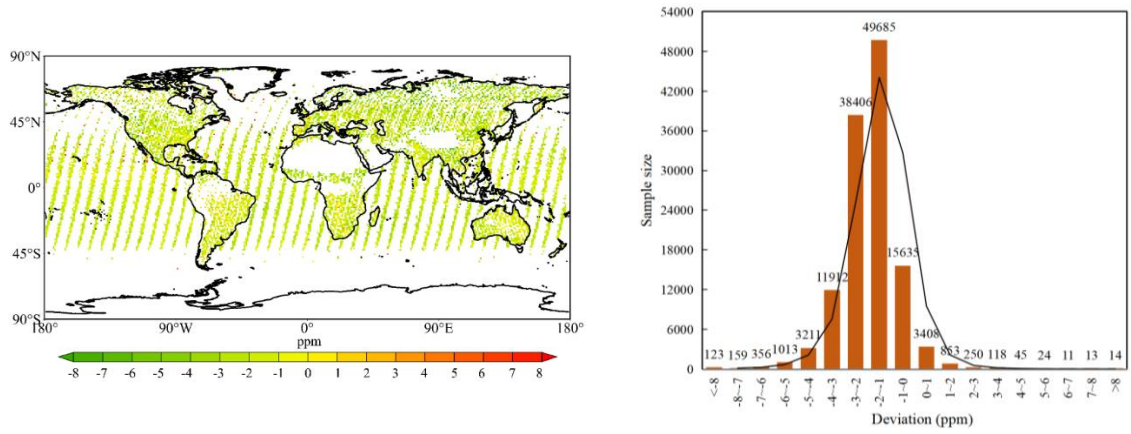

(a) (b)

Figure 1. Deviations from global GOSAT XCO_2 and simulated XCO_2. (a) The deviation distribution diagram, showing the spatial distribution of deviations between the GOSAT-observed XCO_2 (GOSAT XCO_2) and the simulated XCO_2. (b) The deviation histogram, presenting the statistical distribution of these deviations, where the deviation is calculated by subtracting the GOSAT XCO_2 from the simulated XCO_2.

Table 3. Comparison of simulated XCO_2 and GOSAT XCO_2 on a monthly basis.

Time	Sample Size	Simulated Mean (ppm)	Observed Mean (ppm)	Simulated Standard Deviation(ppm)	Observed Standard Deviation(ppm)	RMSE (ppm)	Correlation Coefficient
Jan	6407	385.48	387.24	1.36	1.84	2.15	0.74
Feb	5456	386.03	387.63	1.59	1.92	1.98	0.80
Mar	8285	386.86	388.27	1.88	2.11	1.78	0.86
Apr	8583	387.83	389.27	2.00	2.34	1.81	0.89
May	9396	387.88	389.52	1.74	2.39	2.07	0.86
Jun	10609	386.94	388.90	1.32	1.74	2.39	0.62
Jul	11704	385.47	387.57	2.04	2.07	2.48	0.80
Aug	14258	385.30	387.36	1.64	1.84	2.34	0.81
Sep	14166	385.44	387.51	1.16	1.33	2.33	0.64
Oct	14369	385.97	388.10	0.58	1.14	2.36	0.44
Nov	13207	386.30	388.39	0.42	1.03	2.32	0.28
Dec	8796	386.70	388.78	0.91	1.40	2.35	0.64
Yr	125236	386.26	388.18	1.67	1.89	2.25	0.79

Table 3 presents the total number of samples, mean values of simulated XCO_2 and GOSAT XCO_2, standard deviation (SD), root mean square error (RMSE), and correlation coefficient (r) for each month, providing a comparison of the simulated and observed XCO_2 on a monthly scale. A total of 125,236 observed samples were collected throughout the year. The standard deviations of both simulated and observed XCO_2 exhibited similar trends over the course of the year, and the RMSE for both was below 2.48 ppm. The correlation coefficient for most months exceeded 0.62, with an overall annual correlation coefficient reaching 0.79. In general, the simulated XCO_2 concentrations were 0 to 2.00 ppm lower than the GOSAT XCO_2 concentrations. However, both datasets showed high consistency in terms of spatial and temporal distribution, indicating that the GEOS-Chem simulation results in this study accurately reflect the satellite observation data.

3.1.2. Verification Results of Surface Observation

The simulated surface CO_2 concentrations were derived using the method described in Section 2.3.2 and compared with the CO_2 concentration data from 30 selected NOAA-ESRL surface observation sites. The correlation coefficients between the simulated and observed surface CO_2 concentrations at all sites are shown in Supplementary Information (SI) Figure S1. At more than 90% of the sites, the correlation coefficient exceeded 0.85, and at over half of the sites, it exceeded 0.95. As

 doi:10.20944/preprints202501.2368.v1

shown in Figure 2, CO_2 concentrations at all stations exhibited a general upward trend over the years and displayed different seasonal variations with respect to latitude. Specifically, the observed surface CO_2 concentration in the high latitudes of the Northern Hemisphere, particularly in Europe, showed significant seasonal variation. For example, the annual fluctuation in observed surface CO_2 concentrations at sites such as PAL, HUN, BAL, BSC, BRW, ALT, UUN, and MHD reached about 20 ppm. In contrast, surface CO_2 concentrations in the Southern Hemisphere exhibited smaller fluctuations throughout the year. For example, at sites like USH, BKT, PSA, SEY, ASC, HBA, SYO, and CGO, the annual fluctuation in surface CO_2 concentrations was less than 5 ppm. The simulated surface CO_2 concentrations were highly consistent with those observed at about 80% of the sites, with the mean deviation being less than 2.5 ppm. Overall, the surface CO_2 concentrations simulated by GEOS-Chem in this study align well with the observations from NOAA-ESRL, indicating that the simulation results accurately reflect the spatial and temporal distribution of CO_2 concentrations in the real atmosphere.

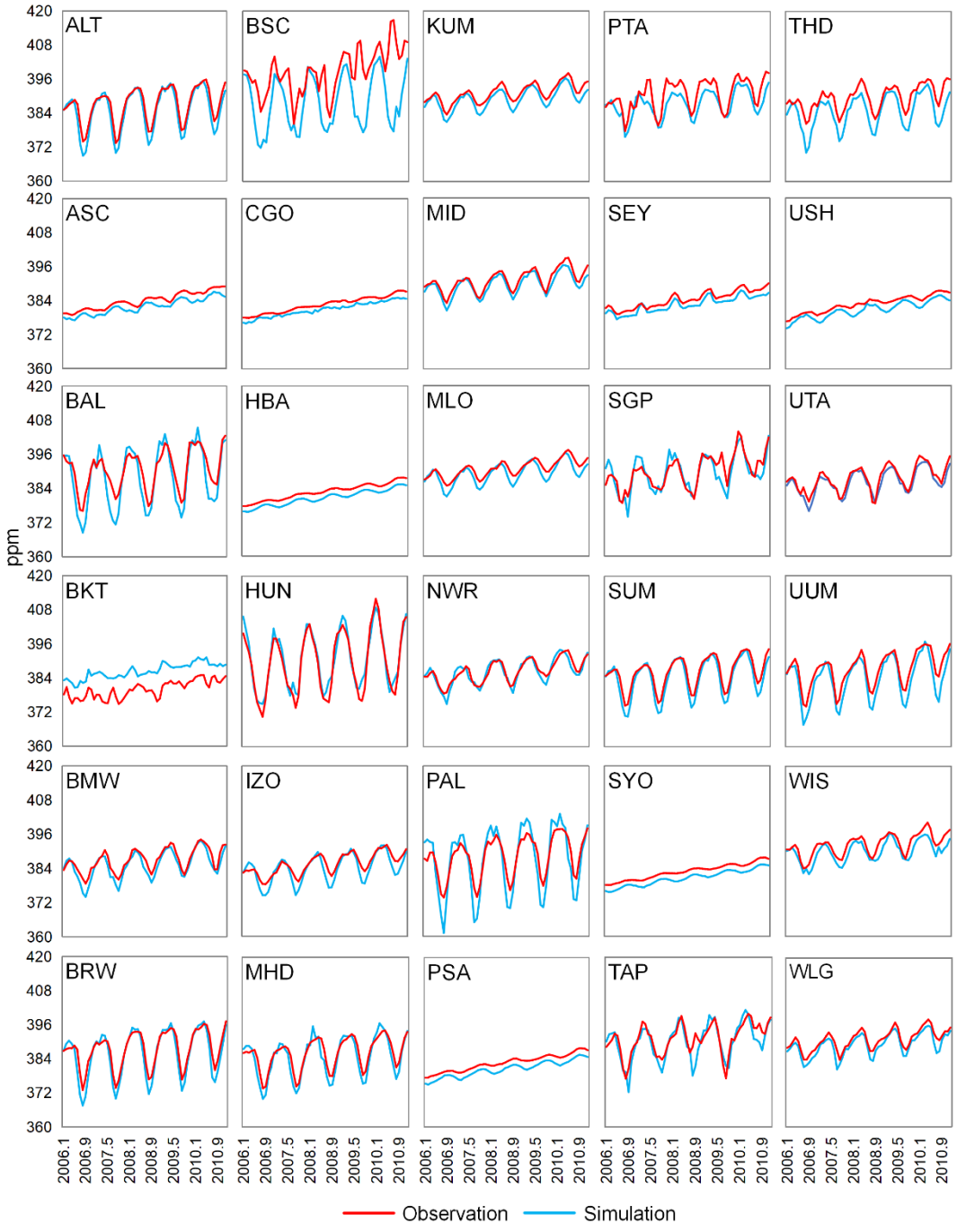

 doi:10.20944/preprints202501.2368.v1

Figure 2. Monthly line charts of simulated and observed surface CO_2 concentrations.

3.2. Temporal and Spatial Characteristics of Global Simulated Atmospheric CO_2 Concentration

The annual average surface CO_2 concentration simulated by GEOS-Chem from 2006 to 2010, as shown in Figure 3 (a), reveals a global average of 383.7 ppm. The data indicate that CO_2 concentrations over land are consistently higher than over the oceans, and concentrations in the Northern Hemisphere exceed those in the Southern Hemisphere. Specifically, CO_2 concentrations in most of the Northern Hemisphere are above 384 ppm, while in the Southern Hemisphere, particularly south of 20°S, CO_2 concentrations generally remain below 382 ppm. These regional variations are primarily influenced by natural factors such as the ocean and terrestrial biosphere, which act as carbon sinks, absorbing some of the CO_2 and thereby lowering atmospheric concentrations. Our study finds that CO_2 concentrations are particularly high in industrialized and densely populated regions such as eastern China, Southeast Asia, northern Eurasia, Europe, and eastern North America, where the average annual CO_2 concentration ranges from 394 to 406 ppm. These findings are consistent with those reported by Miller et al. (2019) [37] and Hamble et al. (2021) [38], who observed that industrialization and high energy consumption lead to elevated CO_2 levels in these areas. Miller et al. (2019) [37] highlighted the role of energy consumption and air pollution in driving high CO_2 concentrations in industrialized regions, a trend that aligns with our own results.

In contrast, CO_2 concentrations in the Southern Hemisphere are generally lower; however, elevated CO_2 levels are observed in northern South America and Central Africa. Specifically, in northern South America, the average annual CO_2 concentration exceeds 398 ppm, and in parts of Central Africa, concentrations can reach over 396 ppm. These findings are in line with Xie et al. (2024) [39], who demonstrated that deforestation, natural gas extraction, and fossil fuel activities are significant contributors to the rise in CO_2 concentrations in these regions. Therefore, while there are notable regional differences in global CO_2 concentrations, these variations are not only driven by natural factors but also by anthropogenic activities such as industrialization, deforestation, and fossil fuel extraction, which is consistent with findings from various studies.

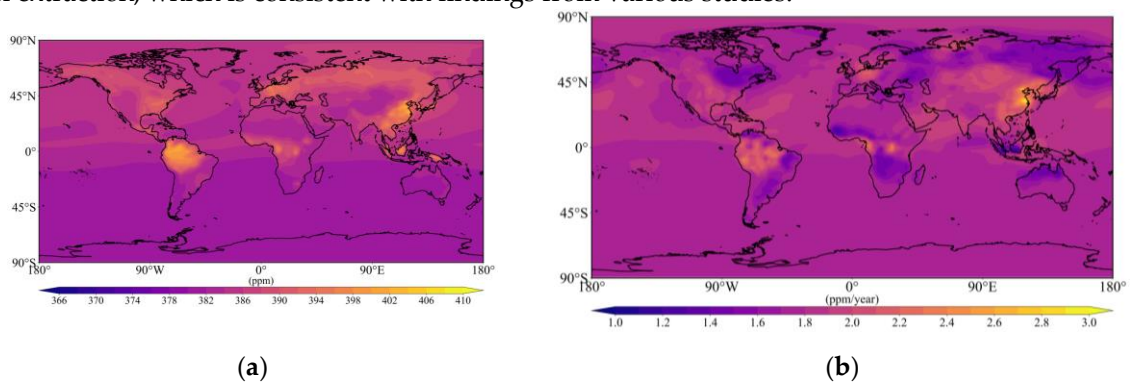

(**a**) (**b**)

Figure 3. (**a**) GEOS-Chem simulated annual surface CO_2 concentration.; (**b**) Average annual growth rate of surface CO_2 concentrations simulated by GEOS-Chem.

As shown in Figure 3 (b), the average annual growth rate of surface CO_2 concentration simulated by GEOS-Chem from 2006 to 2010 is 1.8 ppm year^{-1}. There are significant regional variations in the CO_2 growth rates. Eastern China exhibits the fastest annual increase in CO_2 concentration, with the maximum rate reaching up to 3.0 ppm year^{-1}. This rapid growth is primarily driven by the high population density and intense industrial energy consumption in Eastern China, where industrial emissions are the principal contributor to the accelerated rise in atmospheric CO_2 levels. These findings align with the study by Liu et al. (2024) [40], which underscores the substantial emissions from industrial activities, particularly in densely populated urbanized regions of eastern China. In addition to Eastern China, regions such as Southeastern North America, northern South America, Europe, and Central Africa show annual CO_2 growth rates ranging from 1.8 to 2.4 ppm year^{-1}. These regions also experience elevated industrial emissions, further corroborating the observed higher CO_2 growth rates. However, Southeast Asia stands out with a significantly lower growth rate, averaging around 1.5 ppm year^{-1}, compared to other high-emission regions. This disparity can be attributed to

 doi:10.20944/preprints202501.2368.v1

lower industrial emissions and less intensive energy consumption in Southeast Asia. Research by Liu et al. (2023) [41] suggests that despite rapid industrialization, Southeast Asia still exhibits lower per capita CO_2 emissions compared to regions such as China and North America, leading to a relatively lower growth rate in atmospheric CO_2 concentration.

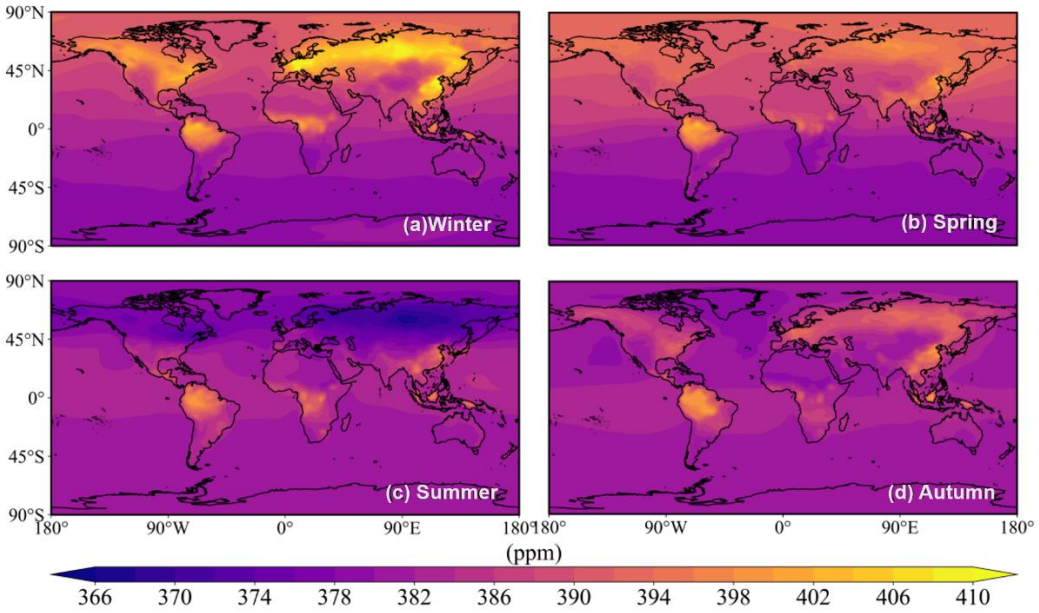

Figure 4. Average annual global surface CO_2 concentrations simulated by GEOS-Chem.

The global distribution of CO_2 concentrations exhibits typical seasonal variation characteristics (Figure 4). Winter is the season with the highest CO_2 concentration of the year, with a global average simulated CO_2 concentration of 385.4 ppm. In regions such as much of Europe, northern Eurasia, and southeastern China, CO_2 concentrations exceed 400 ppm, and in parts of central Europe, central Asia, and eastern China, concentrations even surpass 410 ppm. Summer, on the other hand, is the season with the lowest CO_2 concentration, with a global average simulated CO_2 concentration of 381.5 ppm. During this period, CO_2 concentrations are highest near the equator, ranging from 380 to 400 ppm. North of 45°N, CO_2 concentrations are generally below 380 ppm, and in some areas of central Europe, concentrations can even drop below 370 ppm. The CO_2 concentration in spring and autumn lies between that of winter and summer, with the high-concentration regions showing a distribution similar to that of winter. These seasonal variations can be attributed to changes in temperature and biological activity. In winter, due to lower temperatures and increased heating demands, as well as higher energy consumption in industrialized regions, CO_2 concentrations rise, especially in regions such as eastern China and Europe. In contrast, during the summer, increased photosynthesis by plants leads to significant CO_2 absorption, resulting in lower concentrations, particularly in the higher latitudes of the Northern Hemisphere where vegetation growth and temperature conditions have a suppressive effect on CO_2 levels [42]. Moreover, the CO_2 concentrations in spring and autumn are intermediate, influenced by the combined effects of temperature, plant activity, and climatic conditions [43]. Therefore, seasonal fluctuations are not only a natural consequence of climate changes but also the result of the interplay between biological and human activities, especially in industrialized and energy-intensive areas where CO_2 concentrations fluctuate more significantly.

Figure S2 shows the global average surface CO_2 concentration for each month from 2006 to 2010 as simulated by GEOS-Chem. The global average CO_2 concentration has increased rapidly year by year, and the atmospheric CO_2 concentration has increased by about 7.0 ppm in 5 years. The regression line was obtained by linear fitting of monthly CO_2 concentration, and it can be inferred that the CO_2 concentration increased by about 0.13 ppm per month, and the coefficient of determination reached more than 0.42. In addition, it can be seen from the figure that the global atmospheric average CO_2 concentration has significant seasonal fluctuations.

 doi:10.20944/preprints202501.2368.v1

Figure S3 shows the monthly average global surface CO_2 concentration and growth rate, which is used to further explore the month-to-month variation of global CO_2 concentration. As can be seen from the figure, the global average CO_2 concentration has an obvious seasonal fluctuation cycle, and the global average CO_2 concentration gradually increases from January to March, reaching the annual peak value (389.3 ppm), and then gradually decreases, reaching the annual trough value (383.1 ppm) in August, and the difference of CO_2 concentration in each month of the year is up to 6.2 ppm. In contrast, the month-to-month trend of the growth rate of global mean CO_2 concentration shows an inverse phase change compared with CO_2 concentration. The growth rate of CO_2 concentration in September was the highest (1.95 ppm $year^{-1}$), and the growth rate of CO_2 concentration in February was the lowest (1.62 ppm $year^{-1}$), and the difference of monthly CO_2 concentration growth rate throughout the year was the highest at 0.33 ppm $year^{-1}$.

3.3. Effects of Different CO_2 Sources on Atmospheric CO_2 Concentration

Figure 5 and Table S2 shows the global fluxes of eight different types of CO_2 source sinks simulated by GEOS-Chem in this study. Among them, fossil fuel emissions mainly include CO_2 emissions from natural gas, coal, oil and other fossil fuels. Biomass combustion emissions are mainly CO_2 emissions from forest fires, grassland fires, crop straw burning, household firewood burning, domestic waste burning and so on. Equilibrium biosphere refers to the net ecosystem productivity calculated by the sum of total primary productivity and respiration without considering anthropogenic influence, with seasonal cyclical changes, but the annual net total is 0. Nautical emissions are the emissions caused by Marine navigation activities. Aviation emissions include CO_2 emissions from aviation activities at every layer of the atmosphere. Ocean exchange refers to the amount of CO_2 exchanged between the ocean and the atmosphere. Chemical sources mainly include the oxidation of carbon monoxide, methane and other species into CO_2 in the atmosphere. According to the simulation results, fossil fuel combustion is the world's largest source of CO_2 emissions, emitting 8.81 Gt C $year^{-1}$ into the atmosphere. Biomass combustion is the second largest source of CO_2 emissions globally, emitting 2.00 Gt C $year^{-1}$ into the atmosphere, accounting for about a quarter of fossil fuel emissions. Aviation and navigation emit less than 0.3 Gt C of CO_2 into the atmosphere throughout the year, but as an important source of CO_2 in the atmosphere, their role cannot be ignored. The land and ocean are the most important CO_2 sinks in the world and maintain the dynamic balance of CO_2 in the atmosphere by absorbing CO_2. The land and ocean are the most important CO_2 sinks in the world, and maintain the dynamic balance of CO_2 in the atmosphere by absorbing CO_2.

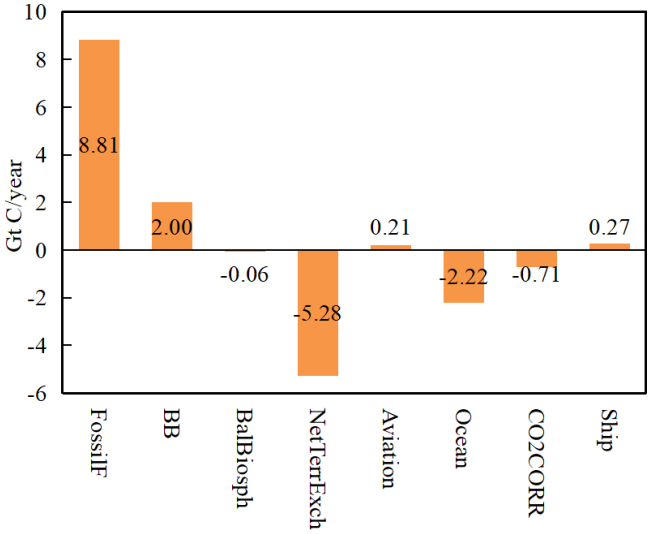

Figure 5. Total global CO_2 fluxes of eight different sources and sinks.

In the process of industrialization and urbanization, global CO_2 emissions from fossil fuels have been increasing over the past few decades. The regional distribution of fossil fuel emissions is uneven, with the largest emitters globally being China, the United States and India, but some small countries

 doi:10.20944/preprints202501.2368.v1

and regions have high per capita emissions. In addition, there are differences in the energy structure of fossil fuels, such as some countries' energy mainly comes from fossil fuels such as coal, while others rely on natural gas, nuclear energy and other energy sources. The burning of fossil fuels releases large amounts of CO_2, far more than other sources of emissions. Global CO_2 emissions from fossil fuels are one of the main causes of climate change, and the CO_2 produced can persist in the atmosphere for decades or even longer, causing global warming and climate crisis, and becoming a global problem [44].

As can be seen from the global distribution of fossil fuel emissions in Figure 6 (a), the high value area of fossil fuel emissions is mainly distributed in the northern Hemisphere, especially in the United States, Europe, India, China and other regions, and the local annual CO_2 emissions can even exceed 2500 g C/m^2. There are also pockets of high fossil fuel emissions along the southeastern coast of South America, Africa and Australia. The spatial distribution of fossil fuel emissions depends on many factors, including geographic location, level of economic development, energy use patterns, industrial structure, population density, and more. Some developed countries and developing countries have a large number of factories and energy consumption facilities, such as power plants and gas stations, national economic development level is high, rapid development, accompanied by high energy consumption. The spatial distribution characteristics of surface atmospheric CO_2 concentration affected by fossil fuel emissions (Figure 6 (b)) are very similar to the spatial distribution characteristics of fossil fuel emissions themselves. The increase in CO_2 concentration caused by fossil fuel emissions is more pronounced in the Northern Hemisphere than in the Southern Hemisphere, which is in contrast to the more intensive population, economic and industrial development in the Northern Hemisphere. Increases in CO_2 concentrations are particularly significant in eastern North America, Europe and eastern Asia. The added value of CO_2 concentration caused by fossil fuel emissions generally exceeds 5 ppm in eastern North America, reaching a maximum of 13 ppm, generally exceeds 7 ppm in Europe, reaching a maximum of about 15 ppm, and generally exceeds 8 ppm in eastern China, reaching a maximum of about 25 ppm.

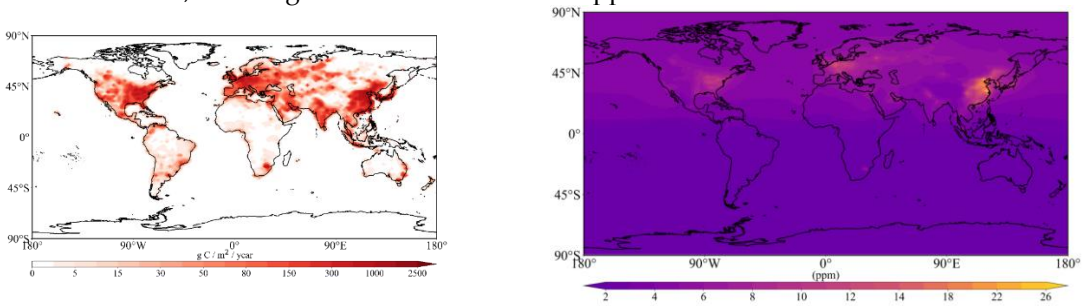

(**a**) (**b**)

Figure 6. (**a**) Fossil fuel carbon emissions; (**b**) Surface atmospheric CO_2 concentrations affected by fossil fuel emissions.

In The Global Carbon Budget 2023 report states that land use change carbon emissions are the second largest source of CO_2 emissions after fossil fuel combustion, of which biomass combustion is an important component. In some developing countries and regions, biomass combustion dominates all sources of carbon emissions [45]. Unlike fossil fuel emissions, CO_2 emitted from biomass combustion is not a new carbon source, but comes from atmospheric CO_2 previously absorbed by plants, so biomass energy is also considered a renewable energy source [46]. Biomass combustion has strong spatial and temporal heterogeneity, showing randomness, periodicity, wide range, multi-point sources, difficult monitoring and other characteristics, and has a very important contribution to the spatial and temporal distribution and dynamic changes of global CO_2. Biomass burning will have an impact on the climate in the short term, but the impact on the climate in the long term is dynamically balanced. However, the problems brought by land use change, water resource consumption, and deforestation still need people's attention.

As can be seen from Figure 7 (a), carbon emissions from biomass combustion are widely distributed globally, particularly in key regions such as Africa, South America, and the Southeast

 doi:10.20944/preprints202501.2368.v1

Asian Peninsula, where it significantly impacts atmospheric CO_2 concentrations. In Africa, biomass burning activities are primarily concentrated in central and southern regions, with annual CO_2 emissions generally exceeding 15 g C/m², and in some areas, surpassing 400 g C/m². This results in an increase in near-surface atmospheric CO_2 concentrations of more than 4.0 ppm throughout the year. These findings identified that biomass burning in Africa and the Amazon Basin leads to similar annual CO_2 concentration increases of up to 4 ppm.

Moreover, this study finds that biomass combustion in central and eastern South America and the Southeast Asian Peninsula also significantly influences local atmospheric CO_2 levels (Figure 7 (b)), with annual CO_2 emissions typically above 25 g C/m², resulting in CO_2 concentration increases exceeding 1.2 ppm. This is consistent with the findings of [47]who reported that biomass burning in Southeast Asia, particularly in Indonesia, can lead to CO_2 concentration increases ranging from 1.5 to 2.0 ppm. Similarly, Andreae and Merlet (2001) [48]provided comparable data, indicating that during fire seasons, CO_2 concentration increases in Africa and South America could reach 3–4 ppm, further validating the observations made in this study.

By comparing these results with existing research, it is evident that the data from this study are in strong agreement with previous findings, reinforcing the significant impact of biomass combustion on global CO_2 concentrations, especially in critical regions like Africa, South America, and Southeast Asia. These findings are crucial for understanding the global carbon cycle and its implications for climate change.

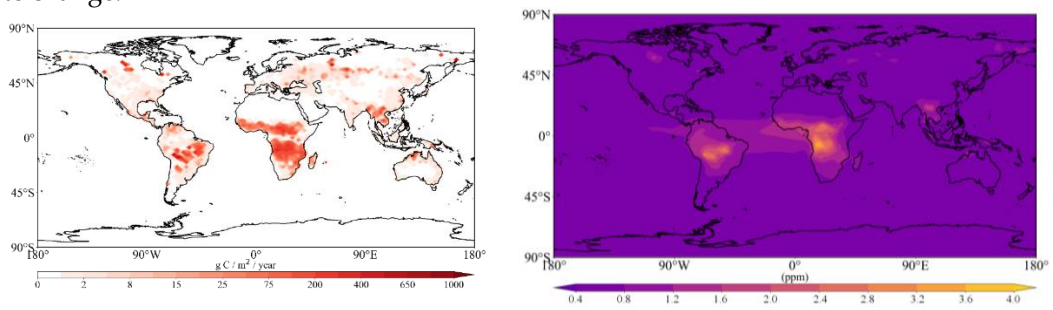

(**a**) (**b**)

Figure 7. (**a**) Carbon emissions from biomass burning; (**b**) Surface atmospheric CO_2 concentration affected by biomass burning emissions.

Influenced by climate change, soil moisture, vegetation growth, soil temperature and land use patterns, CO_2 flux between vegetation and ecosystem has obvious seasonal fluctuations [49]. The equilibrium biosphere exchange flux in the GEOS-Chem model refers to the net difference between the total amount of CO_2 absorbed by plants through photosynthesis and the total amount of ecosystem respiration, which has seasonal characteristics, but the total annual flux remains 0. Specifically, summer is usually the strongest season for CO_2 absorption, because vegetation growth and photosynthesis are enhanced in summer, which increases the absorption of CO_2 from the atmosphere. The strongest release of CO_2 from plants occurs in winter, when vegetation growth slows and soil respiration increases, leading to an increase in CO_2 release into the atmosphere. Based on this feature, this study analyzed the equilibrium biosphere exchange flux and its impact on atmospheric CO_2 concentration on a seasonal scale.

 doi:10.20944/preprints202501.2368.v1

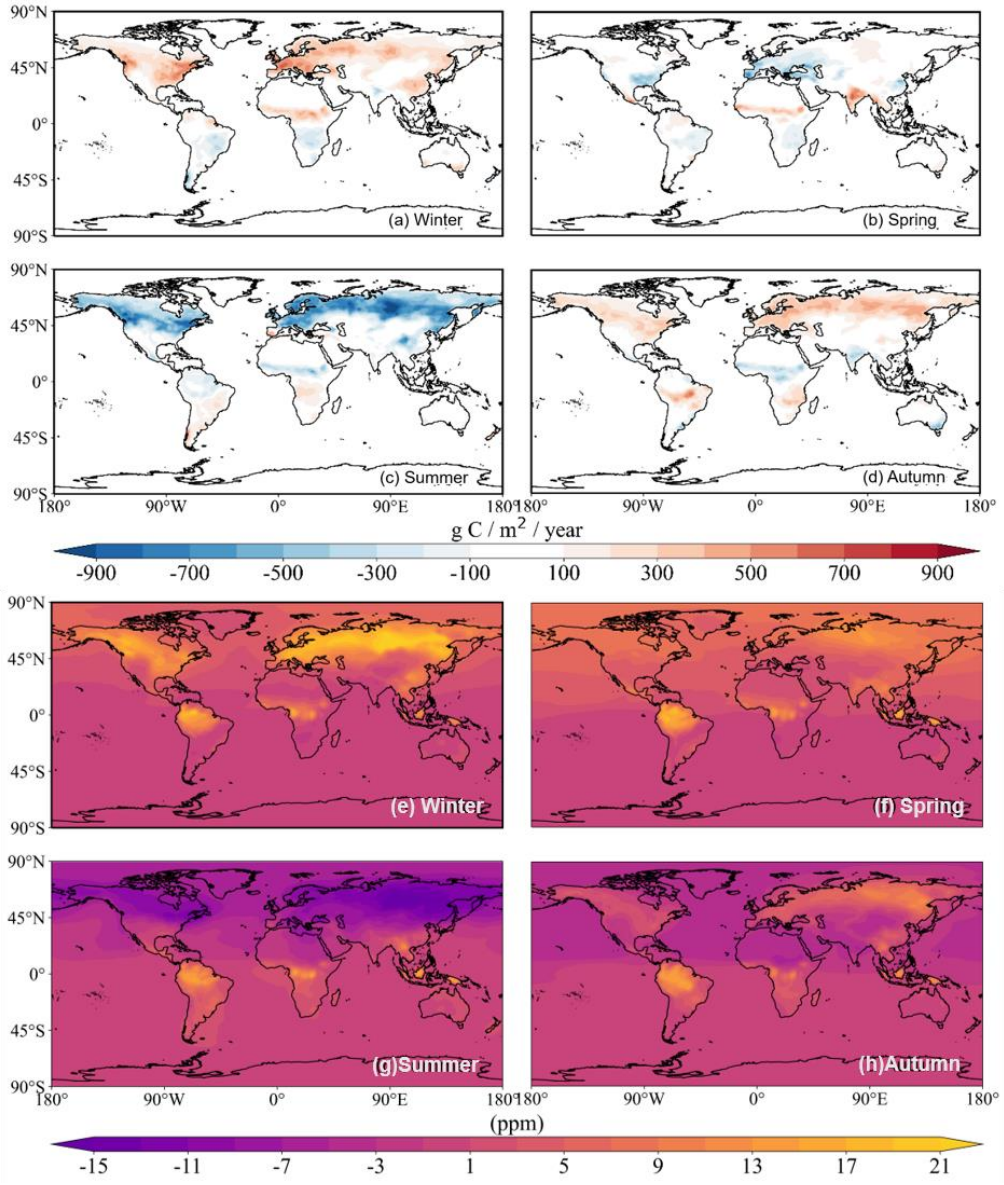

Figure 8. (a)-(d) Balance biosphere carbon flux in four seasons; (e)-(h) Surface atmospheric CO_2 concentrations influenced by balanced biosphere in four seasons.

Figure 8 (a)-(d) shows the equilibrium biosphere exchange carbon flux for the four seasons. Positive values generally represent net CO_2 fluxes from ecosystems to the atmosphere (known as terrestrial carbon sources), and negative values represent net CO_2 removals from the atmosphere to ecosystems (known as terrestrial carbon sinks). Areas where equilibrium biosphere exchange fluxes are prominent coincide highly with areas with dense vegetation, with significant seasonal variations. In winter, the equilibrium biosphere exchange flux is dominated by terrestrial carbon sources in the equatorial regions of South America and Africa, North America, Eurasia except India, and Australia, and peaks in Europe at more than 600 g C/m^2. South of the equator, South America, Africa and India are dominated by terrestrial carbon sinks, and the overall carbon sinks are weak. In summer, terrestrial carbon sinks dominate equatorial regions and the northern hemisphere. The northern Central Asia region has the strongest carbon sink, with local carbon sinks exceeding 900 g C/m^2. The carbon sink in the northern part of North America is also very prominent, generally distributed above 500 g C/m^2. The equilibrium biosphere exchange fluxes in spring and autumn are significantly lower in order of magnitude than in winter and summer, and the distribution of terrestrial carbon sources and carbon pools are also different. It is worth noting that the terrestrial carbon source effect in India is the strongest in the spring, and the whole region is basically more than 300 g C/m^2. The changes of surface atmospheric CO_2 concentration caused by the equilibrium biosphere exchange flux (Figure 8

 doi:10.20944/preprints202501.2368.v1

(e)-(h)) also have seasonal fluctuations. The equilibrium biosphere exchange flux causes a significant increase in atmospheric CO_2 concentration in winter, which is evident in northern and eastern North America, equatorial South America, Africa and Indonesia, northern Eurasia, southeast Asian peninsula and central and eastern China. The increase of CO_2 concentration in Eurasia is generally more than 9 ppm. In summer, the balanced biosphere flux resulted in a general reduction of CO_2 concentrations of more than 7 ppm in continental regions north of 45° N latitude. It is worth noting that the equatorial regions of South America, Africa and Indonesia show an increasing trend of CO_2 caused by the equilibrium biosphere exchange flux throughout the year, which plays a key role in the change of atmospheric CO_2 concentration due to the vigorous growth of vegetation in tropical regions, such as tropical rainforests and savannas.

The net land exchange flux is used to represent the net annual budget or residual amount of CO_2 from the terrestrial biosphere. In the GEOS-Chem model, this partial CO_2 flux is set to a fixed value and divided according to different regions. A total of 11 subregions have been identified on a global scale, and the net land exchange flux within each subregion is nearly consistent. According to Figure 9 (a), Northern North America and South America are the two most typical net terrestrial exchange carbon sources in the world, while other regions are net terrestrial exchange carbon sinks, the top three regions are Southern Africa, Europe and Southern South America. The global net land exchange flux was -5.28 Gt C, dominated by carbon sinks throughout the year. Correspondingly, the surface atmospheric CO_2 concentration affected by the net land exchange flux (Figure 9 (b)) showed similar distribution characteristics, and the overall performance of the whole year was to reduce the atmospheric CO_2 concentration. In northern South America, the change in atmospheric CO_2 concentration due to net land exchange flux was less than 0.8 ppm, and in Europe, the change in atmospheric CO_2 concentration due to net land exchange flux was more than 4.4 ppm.

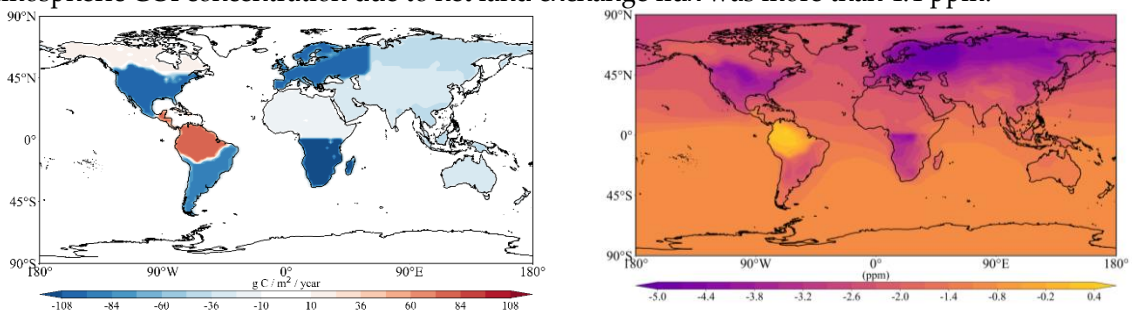

(**a**) (**b**)

Figure 9. (a) Net terrestrial exchange; (b) Surface atmospheric CO_2 concentrations influenced by net terrestrial exchange in four seasons.

Navigation is one of the important sources of greenhouse gas emissions from human activities. According to the third study of greenhouse gas emissions published by the International Maritime Organization (IMO), CO_2 emissions from shipping account for about 2.2% of the total global CO_2 emissions. In 2018, the total CO_2 emissions of the global shipping industry were 1.01 billion tons, of which the CO_2 emissions of maritime transport were 960 million tons, accounting for more than 95%, occupying a dominant position in shipping. CO_2 emissions from land transport and port activities are smaller, at 0.4 million tonnes and 0.1 million tonnes respectively. In addition, CO_2 emissions from the shipping industry continue to grow, with global CO_2 emissions from shipping increasing by 28.9% between 2007 and 2018, with the number of ships increasing by more than 50%. At the same time, the improvement of ship transportation efficiency and fuel utilization rate can only partially offset the increase in emissions caused by the increase in the number of ships [50,51].

Figure 10 (a) shows the spatial distribution of global maritime carbon emissions in 2010. The high value areas of Marine carbon emissions are closely consistent with Marine activities, and the coastal areas and common routes are usually the areas with high CO_2 emissions. This is because these areas usually have a large number of ports and transportation, which requires a large amount of fuel consumption. Maritime CO_2 emissions from European coastal areas are among the highest in the world, exceeding 500 g C/m^2 in some areas. This is because the European region has many ports and

 doi:10.20944/preprints202501.2368.v1

shipping centers, its maritime transport business is large, and the corresponding carbon emissions are relatively high. Secondly, the economic activity of Europe's coastal regions is intensive, including several industries such as manufacturing, trade and tourism, which require a large amount of support from shipping services, further increasing shipping carbon emissions. In addition, the European coastal region has a large maritime fleet, and these vessels often use traditional oil power systems and have relatively high carbon emissions. The spatial distribution of global atmospheric CO_2 concentration increase caused by navigation (Figure 10 (b)) is highly consistent with Marine CO_2 emissions, in which the increase of CO_2 concentration in the northern Hemisphere is significantly higher than that in the Southern Hemisphere, and it is mainly distributed in the two sides of the Atlantic and Pacific oceans. Coastal areas in northern Germany and Denmark have the highest CO_2 increases in the world, with local CO_2 increases from Marine CO_2 emissions reaching up to 0.48 ppm or more.

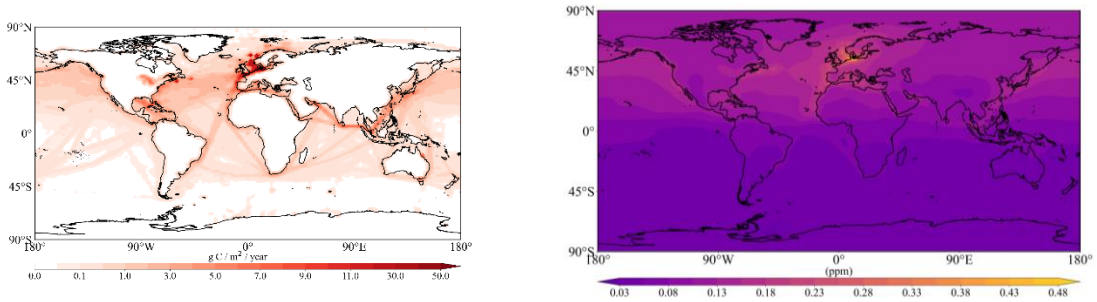

(**a**) (**b**)

Figure 10. (**a**) Carbon emissions from ship; (**b**) Surface atmospheric CO_2 concentrations affected by ship emissions.

Aviation activities are a significant source of global greenhouse gas emissions. The bulk of aviation's carbon emissions come from CO_2 produced by burning fuel in jet engines. According to the International Civil Aviation Organization (ICAO), CO_2 emissions from aviation account for about 2–3% of total global CO_2 emissions. Carbon emissions from aviation have grown over the past few decades and are expected to continue to increase in the future. The International Energy Agency (IEA), based on future economic growth and expansion of the aviation industry, as well as technology and policy measures for the aviation industry in the future, predicts that global carbon emissions from the aviation industry could grow 2–3 times by 2040. IEA 2023 report, "The Future of Petrochemicals: Towards more sustainable plastics and fertilisers" Long-haul international flights have relatively high carbon emissions because they use more fuel. Short-haul flights have relatively low carbon emissions. In addition, the impact of CO_2 emitted at high altitude on climate change is more significant than that of CO_2 emitted at ground level. This is because, in addition to ground airports, aviation carbon emissions mainly occur at high altitude, high-altitude CO_2 emissions can be more easily dispersed around the world, and its greenhouse effect is more intense at high altitude. For example, the Fifth Assessment report released by the United Nations Intergovernmental Panel on Climate Change (IPCC) pointed out that the contribution of carbon emissions from aviation activities to global warming is about 3.5–4.9%.

Affected by many factors such as flight route, flight speed, aircraft type and meteorological conditions, the height of aviation carbon emissions is not fixed. Figure 11 (a) shows the aggregate CO_2 emissions from aviation at each vertical level of the atmosphere. Aviation CO_2 emissions are highly consistent with airport locations, showing the locations of major global air terminals. Among them, the United States, Europe, southeast China and Japan are the regions with the highest emissions of global aviation, with emissions reaching more than 20 g C/m^2. In addition, the distribution of aviation emissions is closely related to the route, and this part comes from the CO_2 emitted by the aircraft during flight. Unlike other sources of emissions, aviation CO_2 emissions occur at both surface and high altitudes, and at different altitudes in different parts of the world. Therefore, this study explores the impact of aviation emissions on the average atmospheric CO_2 concentration at each layer. As can be seen from Figure 11 (b), the increase in the mean atmospheric CO_2

 doi:10.20944/preprints202501.2368.v1

concentration of each layer caused by aviation CO_2 emissions is higher in the northern Hemisphere and lower in the Southern Hemisphere. Due to the enhanced mixing in the upper atmosphere, the distribution of CO_2 concentration is zonally uniform across the globe, with a north-south gradient of about 0.04 ppm. At the same time, this study also explored the changes in surface atmospheric CO_2 concentration affected by aviation CO_2 emissions in 2010 (Figure S4). The increase of surface CO_2 concentration was also high in the northern Hemisphere and low in the Southern Hemisphere, but it was prominent in the continental region. Among them, the United States and Europe are the two major regions where the surface atmospheric CO_2 concentration increased significantly due to aviation CO_2 emissions, and the local CO_2 concentration increase value can reach more than 0.1 ppm, and it is one-to-one corresponding to the airport location.

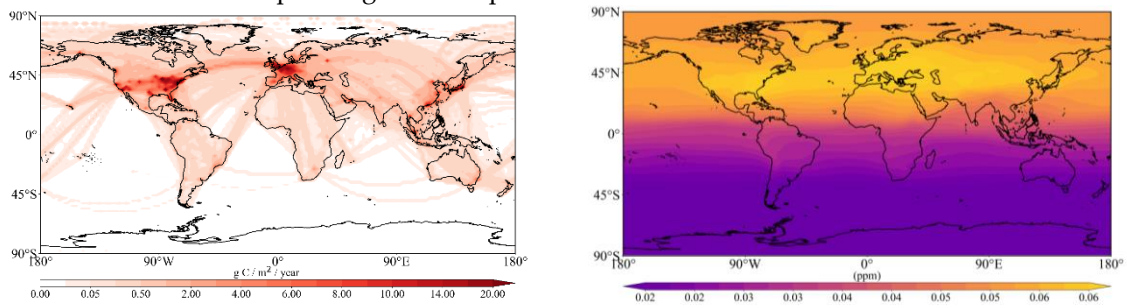

(**a**) (**b**)

Figure 11. (**a**) Carbon emissions from aviation; (**b**) Average atmospheric CO_2 concentrations from different layers affected by aviation emissions.

CO_2 exchange between the ocean and atmosphere is one of the important processes affecting the global carbon cycle and one of the important factors affecting global climate change. Overall, the ocean, as a major global carbon sink, absorbs about 25% of CO_2 emissions from the atmosphere, which plays an important role in regulating climate and mitigating the greenhouse effect [52]. In tropical areas, the temperature of the sea surface is higher, and these areas usually have a greater amount of sunlight. As a result, the oceans in these areas typically release CO_2; In polar sea regions, sea surface temperatures are cooler, and the amount of sunlight in these regions is generally less. As a result, the oceans in these regions typically absorb CO_2 [53]. The rate at which the ocean absorbs CO_2 from the atmosphere varies with the seasons, with a faster rate in winter and a slower rate in summer. The surface of the ocean is the main area of CO_2 absorption and release, and the deep ocean usually has relatively high CO_2 concentrations. Ocean circulation also has an important effect on the exchange of CO_2 between the ocean and the atmosphere. For example, ocean circulation around Antarctica typically results in the release of large amounts of CO_2 from the region's oceans [54].

Figure 12 (a) shows the global ocean exchange carbon flux, representing the exchange of CO_2 between the ocean and the atmosphere. Positive values indicate that CO_2 enters the atmosphere from the ocean, that is, the ocean emits CO_2 (Marine CO_2 source); Negative values represent the passage of CO_2 from the atmosphere into the ocean, i.e. the uptake of CO_2 by the ocean (ocean CO_2 sink). As can be seen from the figure 12 (a), the tropical region and the circumantarctic region are the main sources of ocean CO_2 exchange in the world, among which the tropical eastern Pacific region and the junction of the Arabian Sea and the Gulf of Aden are the regions with the strongest annual Marine CO_2 emission, with a local maximum of more than 36 g C/m^2. The Norwegian Sea and Labrador Bay near the Arctic Circle are the two regions with the strongest annual Marine CO_2 absorption, with local CO_2 absorption fluxes reaching above 54 g C/m^2. As can be seen from Figure 12 (b), the impact of ocean exchange on surface atmospheric CO_2 concentration is mainly manifested as the reduction of global CO_2 concentration. Specifically, changes in CO_2 concentrations at the ocean surface decrease from the equator to the poles. The annual ocean exchange flux decreased the CO_2 concentration in the equatorial waters by 0~0.8 ppm. The CO_2 concentration in the sea area near 45° S latitude decreased by 1.1~1.5 ppm; The CO_2 concentration in the North Atlantic Ocean to the south of the Arctic Ocean decreased by more than 1.2 ppm, of which the highest CO_2 concentration in the east and south of Greenland exceeded 1.6 ppm.

 doi:10.20944/preprints202501.2368.v1

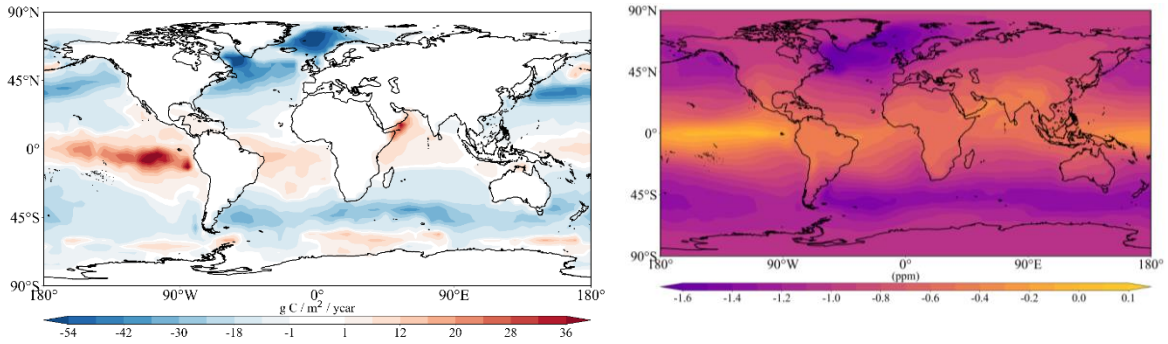

(**a**) (**b**)

Figure 12. (**a**) Ocean exchange carbon fluxes; (**b**) Surface atmospheric CO_2 concentrations influenced by ocean exchange.

The CO_2 emission inventory in the traditional atmospheric model ignores the CO_2 produced by oxidation of other carbon species. This simulation process has defects and lacks comprehensive consideration of the CO_2 generation process, which will lead to inaccurate simulation results. In order to more accurately simulate global atmospheric CO_2 levels, Nassar et al (2010) [55] improved the CO_2 emission inventory of the GEOS-Chem model to take into account CO_2 produced by oxidation of other carbon species, such as biomass burning, land use change, and forest harvesting. In addition, there are other carbon species that may produce CO_2, such as weathering of carbonate rocks and respiration of aquatic organisms. These oxidation effects can lead to the release of CO_2 into the atmosphere, which has an impact on global climate change. Taking into account the chemical source flux of CO_2 produced by the oxidation of carbon species, the model can more accurately simulate global atmospheric CO_2 levels and provide more accurate data to guide the development and implementation of global climate change policies.

As can be seen from Figure 13 (a), the CO_2 generated by oxidation of other species is subtracted in the simulation, that is, the model simulation results are corrected. The flux of chemical sources is widely distributed globally, which is the result of the comprehensive action of multiple processes and species oxidation of CO_2 in the region. Eastern North America, South America, Europe, Central Africa, South Asia, and Southeast Asia are several regions with large chemical source fluxes Figure 13 (b), which are basically above 10 g C/m^2. The variation of surface CO_2 concentration affected by chemical source flux is very consistent with the distribution of chemical source flux, which is mainly manifested by reducing and correcting the simulated CO_2 concentration. Chemical source fluxes widely cause CO_2 concentration changes on a global scale, among which, central Africa and eastern China are the regions most affected by chemical source fluxes, and the maximum annual CO_2 concentration change can exceed 1.0 ppm, which is closely related to a large number of biomass burning. In addition, in eastern North America, South America, northern Africa, Europe, Asia and Southeast Asia, the CO_2 concentration change value is basically above 0.25 ppm.

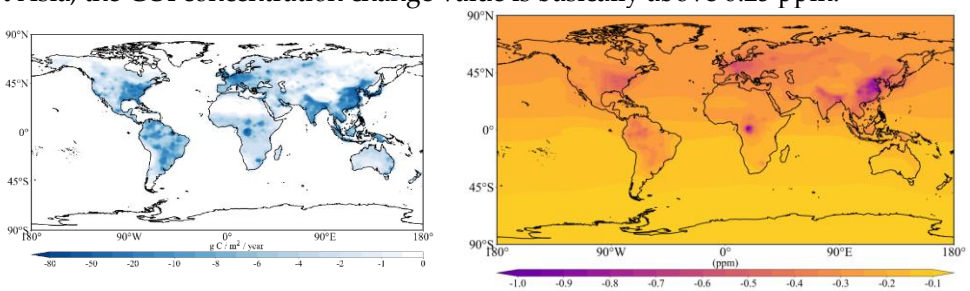

(**a**) (**b**)

Figure 13. (**a**) Chemical sources carbon fluxes; (**b**) Surface atmospheric CO_2 concentrations influenced by chemical sources

4. Conclusions

 doi:10.20944/preprints202501.2368.v1

The study shows that fossil fuel combustion is the largest source of atmospheric CO_2 emissions, reaching 8.81 Gt C/year, and biomass combustion is the second largest source of CO_2 emissions, reaching about a quarter of fossil fuel combustion in 2010, reaching 2.00 Gt C/year. In addition, aviation emissions, Marine emissions, chemical reactions also have a greater contribution to atmospheric CO_2 emissions. The ocean is a very important sink of atmospheric CO_2, absorbing 2.22 Gt C/year from the atmosphere, and the terrestrial biosphere is also an important sink of atmospheric CO_2, with a net terrestrial ecosystem exchange of 5.28 Gt C/year.

The influence of different CO_2 source flux on atmospheric CO_2 concentration is highly correlated with the spatial distribution and flux magnitude of CO_2 source flux, and is highly consistent in spatial distribution. Specifically: Emissions from fossil fuel combustion are significantly greater in the Northern Hemisphere than in the southern Hemisphere, with particularly large emissions in the eastern United States, Europe, East Asia, and India. Global emissions from fossil fuel combustion have caused the increase in atmospheric CO_2 concentration, and fossil fuel combustion in the northern hemisphere has a greater impact on atmospheric CO_2, and the largest contribution is in eastern China. CO_2 emissions from biomass combustion are widely distributed in the world, and Africa is the land region that contributes the most to global biomass combustion emissions. The spatial distribution of CO_2 concentration increase caused by biomass combustion emission is similar to that of biomass combustion emission itself. Among them, South America, Africa and Southeast Asian peninsula are the three regions most affected by biomass combustion emissions, and the increase of CO_2 concentration is particularly obvious. The seasonal variation of atmospheric CO_2 source and sink caused by the equilibrium biosphere also resulted in the corresponding seasonal variation of atmospheric CO_2 concentration. In summer, the equilibrium biosphere reduces the atmospheric CO_2 concentration in the northern Hemisphere and increases the atmospheric CO_2 concentration in some parts of the Southern hemisphere. North America and the northern part of South America are two typical net terrestrial exchange carbon sources in the world, while the other regions are net terrestrial exchange carbon sinks. The net terrestrial exchange flux has corresponding effects on atmospheric CO_2 concentration, and the spatial distribution characteristics correspond to the net terrestrial exchange flux. Aviation and maritime activities are important sources of global atmospheric CO_2 emissions. Aviation emissions and maritime emissions are mainly concentrated on their respective routes, as well as airports for aircraft and ports for ships. The spatial distribution of global atmospheric CO_2 concentration increase caused by aviation emissions and maritime emissions corresponds to the spatial distribution of CO_2 emissions themselves. The ocean is primarily a sink for atmospheric CO_2. The tropical region and the circumantarctic region are the main global sources of ocean CO_2 exchange, and the Norwegian Sea and Labrador Bay near the Arctic Circle are the two regions with the strongest ocean CO_2 absorption throughout the year. The impact of ocean exchange on surface atmospheric CO_2 concentration is mainly manifested in the reduction of global CO_2 concentration. Atmospheric CO_2 chemical reaction sources are widely distributed around the world and are mainly used to quantify the oxidation of carbon species to produce CO_2. The effect of chemical sources on atmospheric CO_2 concentration is mainly used to reduce the simulated CO_2 concentration in the model. China and Central Africa are the regions with the strongest chemical reaction sources.

Supplementary Materials: This supplementary document contains Figure S1-Figure S4, Table S1-Table S2.

Author Contributions: Conceptualization, G.Q. and Y.S.; Data curation, Y.Y. and M.S.; Formal analysis, M.S.; Funding acquisition, J.Z.; Investigation, G.Q., W.W. and Z.Z.; Methodology, Y.S.; Project administration, J.Z. and Y.S.; Resources, M.S.; Software, Y.Y.; Supervision, Y.S.; Validation, W.W. and Z.Z.; Visualization, Y.Y.; Writing – original draft, G.Q.; Writing – review & editing, G.Q. and Y.Y. All authors have read and agreed to the published version of the manuscript.

Funding: This research is supported by the National Key Research and Development Program of China (2023YFB3907404), the FY-3 Lot 03 Meteorological Satellite Engineering Ground Application System Ecological Monitoring and Assessment Application Project Phase I (ZQC-R22227), the National Natural Science Foundation of China (42071398), the Heilongjiang Provincial Natural Science Foundation (PL2024D013) and the Academic Innovation Project of Harbin Normal University (HSDBSCX2021-104).

Data Availability Statement: Data of the results of this study can be obtained upon request.

Acknowledgments: We would like to express our sincere gratitude to Researcher Yu-Sheng Shi and Professor Jia Zhou for their invaluable guidance in shaping the framework of this paper. Special thanks to Yongliang Liang and Mengqian Su for their diligent work on data analysis and detail modifications. We also appreciate the support from the Institute of Space and Astronautical Information Innovation, Chinese Academy of Sciences, in building the information platform.

Conflicts of Interest: The authors declare no conflicts of interest.

References

1. Friedlingstein, P.; O'Sullivan, M.; Jones, M.W.; Andrew, R.M.; Hauck, J.; Landschützer, P.; Le Quéré, C.; Li, H.; Luijkx, I.T.; Olsen, A.; et al. Global Carbon Budget 2024 **2024**.
2. Bauska, T.K.; Joos, F.; Mix, A.C.; Roth, R.; Ahn, J.; Brook, E.J. Links between Atmospheric Carbon Dioxide, the Land Carbon Reservoir and Climate over the Past Millennium. *Nat Geosci* **2015**, *8*, 383–387, doi:10.1038/ngeo2422.
3. Keenan, T.F.; Prentice, I.C.; Canadell, J.G.; Williams, C.A.; Wang, H.; Raupach, M.; Collatz, G.J. Recent Pause in the Growth Rate of Atmospheric CO_2 Due to Enhanced Terrestrial Carbon Uptake. *Nat Commun* **2016**, *7*, 13428, doi:10.1038/ncomms13428.
4. Kukkonen, J.; Olsson, T.; Schultz, D.M.; Baklanov, A.; Klein, T.; Miranda, A.I.; Monteiro, A.; Hirtl, M.; Tarvainen, V.; Boy, M.; et al. A Review of Operational, Regional-Scale, Chemical Weather Forecasting Models in Europe. *Atmos Chem Phys* **2012**, *12*, 1–87, doi:10.5194/acp-12-1-2012.
5. Feng, L.; Palmer, P.I.; Yang, Y.; Yantosca, R.M.; Kawa, S.R.; Paris, J.-D.; Matsueda, H.; Machida, T. Evaluating a 3-D Transport Model of Atmospheric CO_2 Using Ground-Based, Aircraft, and Space-Borne Data. *Atmos Chem Phys* **2011**, *11*, 2789–2803, doi:10.5194/acp-11-2789-2011.
6. Zeng, N.; Han, P.; Liu, Z.; Liu, D.; Oda, T.; Martin, C.; Liu, Z.; Yao, B.; Sun, W.; Wang, P.; et al. Global to Local Impacts on Atmospheric CO_2 from the COVID-19 Lockdown, Biosphere and Weather Variabilities. *Environmental Research Letters* **2022**, *17*, 015003, doi:10.1088/1748-9326/ac3f62.
7. Suntharalingam, P.; Spivakovsky, C.M.; Logan, J.A.; McElroy, M.B. Estimating the Distribution of Terrestrial CO_2 Sources and Sinks from Atmospheric Measurements: Sensitivity to Configuration of the Observation Network. *Journal of Geophysical Research: Atmospheres* **2003**, *108*, doi:10.1029/2002JD002207.
8. Nassar, R.; Jones, D.B.A.; Suntharalingam, P.; Chen, J.M.; Andres, R.J.; Wecht, K.J.; Yantosca, R.M.; Kulawik, S.S.; Bowman, K.W.; Worden, J.R.; et al. Modeling Global Atmospheric CO_2 with Improved Emission Inventories and CO_2 Production from the Oxidation of Other Carbon Species. *Geosci Model Dev* **2010**, *3*, 689–716, doi:10.5194/gmd-3-689-2010.
9. Randerson, J.T.; Thompson, M. V.; Conway, T.J.; Fung, I.Y.; Field, C.B. The Contribution of Terrestrial Sources and Sinks to Trends in the Seasonal Cycle of Atmospheric Carbon Dioxide. *Global Biogeochem Cycles* **1997**, *11*, 535–560, doi:10.1029/97GB02268.
10. Suntharalingam, P.; Jacob, D.J.; Palmer, P.I.; Logan, J.A.; Yantosca, R.M.; Xiao, Y.; Evans, M.J.; Streets, D.G.; Vay, S.L.; Sachse, G.W. Improved Quantification of Chinese Carbon Fluxes Using CO_2 /CO Correlations in Asian Outflow. *Journal of Geophysical Research: Atmospheres* **2004**, *109*, doi:10.1029/2003JD004362.
11. Nassar, R.; Jones, D.B.A.; Suntharalingam, P.; Chen, J.M.; Andres, R.J.; Wecht, K.J.; Yantosca, R.M.; Kulawik, S.S.; Bowman, K.W.; Worden, J.R.; et al. Modeling Global Atmospheric CO_2 with Improved Emission Inventories and CO_2 Production from the Oxidation of Other Carbon Species. *Geosci Model Dev* **2010**, *3*, 689–716, doi:10.5194/gmd-3-689-2010.
12. Gelaro, R.; McCarty, W.; Suárez, M.J.; Todling, R.; Molod, A.; Takacs, L.; Randles, C.A.; Darmenov, A.; Bosilovich, M.G.; Reichle, R.; et al. The Modern-Era Retrospective Analysis for Research and Applications, Version 2 (MERRA-2). *J Clim* **2017**, *30*, 5419–5454, doi:10.1175/JCLI-D-16-0758.1.
13. Koster R D, D.A.S. da S.A.M. The Quick Fire Emissions Dataset (QFED): Documentation of Versions 2.1, 2.2 and 2.4[R]; 2015;
14. Oda, T.; Maksyutov, S. A Very High-Resolution (1 Km×1 Km) Global Fossil Fuel CO_2 Emission Inventory Derived Using a Point Source Database and Satellite Observations of Nighttime Lights. *Atmos Chem Phys* **2011**, *11*, 543–556, doi:10.5194/acp-11-543-2011.

15. Takahashi, T.; Sutherland, S.C.; Wanninkhof, R.; Sweeney, C.; Feely, R.A.; Chipman, D.W.; Hales, B.; Friederich, G.; Chavez, F.; Sabine, C.; et al. Climatological Mean and Decadal Change in Surface Ocean PCO_2, and Net Sea–Air CO_2 Flux over the Global Oceans. *Deep Sea Research Part II: Topical Studies in Oceanography* **2009**, *56*, 554–577, doi:10.1016/j.dsr2.2008.12.009.
16. Messerschmidt, J.; Parazoo, N.; Wunch, D.; Deutscher, N.M.; Roehl, C.; Warneke, T.; Wennberg, P.O. Evaluation of Seasonal Atmosphere–Biosphere Exchange Estimations with TCCON Measurements. *Atmos Chem Phys* **2013**, *13*, 5103–5115, doi:10.5194/acp-13-5103-2013.
17. Baker, D.F.; Law, R.M.; Gurney, K.R.; Rayner, P.; Peylin, P.; Denning, A.S.; Bousquet, P.; Bruhwiler, L.; Chen, Y. -H.; Ciais, P.; et al. TransCom 3 Inversion Intercomparison: Impact of Transport Model Errors on the Interannual Variability of Regional CO_2 Fluxes, 1988–2003. *Global Biogeochem Cycles* **2006**, *20*, doi:10.1029/2004GB002439.
18. Hoesly, R.M.; Smith, S.J.; Feng, L.; Klimont, Z.; Janssens-Maenhout, G.; Pitkanen, T.; Seibert, J.J.; Vu, L.; Andres, R.J.; Bolt, R.M.; et al. Historical (1750–2014) Anthropogenic Emissions of Reactive Gases and Aerosols from the Community Emissions Data System (CEDS). *Geosci Model Dev* **2018**, *11*, 369–408, doi:10.5194/gmd-11-369-2018.
19. Olsen, S.C.; Brasseur, G.P.; Wuebbles, D.J.; Barrett, S.R.H.; Dang, H.; Eastham, S.D.; Jacobson, M.Z.; Khodayari, A.; Selkirk, H.; Sokolov, A.; et al. Comparison of Model Estimates of the Effects of Aviation Emissions on Atmospheric Ozone and Methane. *Geophys Res Lett* **2013**, *40*, 6004–6009, doi:10.1002/2013GL057660.
20. Nassar, R.; Jones, D.B.A.; Suntharalingam, P.; Chen, J.M.; Andres, R.J.; Wecht, K.J.; Yantosca, R.M.; Kulawik, S.S.; Bowman, K.W.; Worden, J.R.; et al. Modeling Global Atmospheric CO_2 with Improved Emission Inventories and CO_2 Production from the Oxidation of Other Carbon Species. *Geosci Model Dev* **2010**, *3*, 689–716, doi:10.5194/gmd-3-689-2010.
21. Fu, Y.; Liao, H.; Tian, X.; Gao, H.; Jia, B.; Han, R. Impact of Prior Terrestrial Carbon Fluxes on Simulations of Atmospheric CO_2 Concentrations. *Journal of Geophysical Research: Atmospheres* **2021**, *126*, doi:10.1029/2021JD034794.
22. Reddington, C.L.; Conibear, L.; Robinson, S.; Knote, C.; Arnold, S.R.; Spracklen, D. V. Air Pollution From Forest and Vegetation Fires in Southeast Asia Disproportionately Impacts the Poor. *Geohealth* **2021**, *5*, doi:10.1029/2021GH000418.
23. Gao, M.; Beig, G.; Song, S.; Zhang, H.; Hu, J.; Ying, Q.; Liang, F.; Liu, Y.; Wang, H.; Lu, X.; et al. The Impact of Power Generation Emissions on Ambient PM2.5 Pollution and Human Health in China and India. *Environ Int* **2018**, *121*, 250–259, doi:10.1016/j.envint.2018.09.015.
24. Kou, X.; Zhang, M.; Peng, Z.; Wang, Y. Assessment of the Biospheric Contribution to Surface Atmospheric CO_2 Concentrations over East Asia with a Regional Chemical Transport Model. *Adv Atmos Sci* **2015**, *32*, 287–300, doi:10.1007/s00376-014-4059-6.
25. Jing, Y.; Wang, T.; Zhang, P.; Chen, L.; Xu, N.; Ma, Y. Global Atmospheric CO_2 Concentrations Simulated by GEOS-Chem: Comparison with GOSAT, Carbon Tracker and Ground-Based Measurements. *Atmosphere (Basel)* **2018**, *9*, 175, doi:10.3390/atmos9050175.
26. Wunch, D.; Toon, G.C.; Blavier, J.-F.L.; Washenfelder, R.A.; Notholt, J.; Connor, B.J.; Griffith, D.W.T.; Sherlock, V.; Wennberg, P.O. The Total Carbon Column Observing Network. *Philosophical Transactions of the Royal Society A: Mathematical, Physical and Engineering Sciences* **2011**, *369*, 2087–2112, doi:10.1098/rsta.2010.0240.
27. Karbasi, S.; Malakooti, H.; Rahnama, M.; Azadi, M. Study of Mid-Latitude Retrieval XCO_2 Greenhouse Gas: Validation of Satellite-Based Shortwave Infrared Spectroscopy with Ground-Based TCCON Observations. *Science of The Total Environment* **2022**, *836*, 155513, doi:10.1016/j.scitotenv.2022.155513.
28. Cogan, A.J.; Boesch, H.; Parker, R.J.; Feng, L.; Palmer, P.I.; Blavier, J. -F. L.; Deutscher, N.M.; Macatangay, R.; Notholt, J.; Roehl, C.; et al. Atmospheric Carbon Dioxide Retrieved from the Greenhouse Gases Observing SATellite (GOSAT): Comparison with Ground-based TCCON Observations and GEOS-Chem Model Calculations. *Journal of Geophysical Research: Atmospheres* **2012**, *117*, doi:10.1029/2012JD018087.

29. Lindqvist, H.; O'Dell, C.W.; Basu, S.; Boesch, H.; Chevallier, F.; Deutscher, N.; Feng, L.; Fisher, B.; Hase, F.; Inoue, M.; et al. Does GOSAT Capture the True Seasonal Cycle of Carbon Dioxide? *Atmos Chem Phys* **2015**, *15*, 13023–13040, doi:10.5194/acp-15-13023-2015.
30. Morino, I.; Uchino, O.; Inoue, M.; Yoshida, Y.; Yokota, T.; Wennberg, P.O.; Toon, G.C.; Wunch, D.; Roehl, C.M.; Notholt, J.; et al. Preliminary Validation of Column-Averaged Volume Mixing Ratios of Carbon Dioxide and Methane Retrieved from GOSAT Short-Wavelength Infrared Spectra 2010.
31. Connor, B.J.; Boesch, H.; Toon, G.; Sen, B.; Miller, C.; Crisp, D. Orbiting Carbon Observatory: Inverse Method and Prospective Error Analysis. *Journal of Geophysical Research: Atmospheres* **2008**, *113*, doi:10.1029/2006JD008336.
32. Masarie, K.A.; Peters, W.; Jacobson, A.R.; Tans, P.P. ObsPack: A Framework for the Preparation, Delivery, and Attribution of Atmospheric Greenhouse Gas Measurements. *Earth Syst Sci Data* **2014**, *6*, 375–384, doi:10.5194/essd-6-375-2014.
33. Fu, Y.; Liao, H.; Tian, X.-J.; Gao, H.; Cai, Z.-N.; Han, R. Sensitivity of the Simulated CO_2 Concentration to Inter-Annual Variations of Its Sources and Sinks over East Asia. *Advances in Climate Change Research* **2019**, *10*, 250–263, doi:10.1016/j.accre.2020.03.001.
34. Li, R.; Zhang, M.; Chen, L.; Kou, X.; Skorokhod, A. CMAQ Simulation of Atmospheric CO_2 Concentration in East Asia: Comparison with GOSAT Observations and Ground Measurements. *Atmos Environ* **2017**, *160*, 176–185, doi:10.1016/j.atmosenv.2017.03.056.
35. Fu, Y.; Liao, H.; Tian, X.; Gao, H.; Jia, B.; Han, R. Impact of Prior Terrestrial Carbon Fluxes on Simulations of Atmospheric CO_2 Concentrations. *Journal of Geophysical Research: Atmospheres* **2021**, *126*, doi:10.1029/2021JD034794.
36. Chen, Z.H.; Zhu, J.; Zeng, N. Improved Simulation of Regional CO_2 Surface Concentrations Using GEOS-Chem and Fluxes from VEGAS. *Atmos Chem Phys* **2013**, *13*, 7607–7618, doi:10.5194/acp-13-7607-2013.
37. Deryugina, T.; Heutel, G.; Miller, N.H.; Molitor, D.; Reif, J. The Mortality and Medical Costs of Air Pollution: Evidence from Changes in Wind Direction. *American Economic Review* **2019**, *109*, 4178–4219, doi:10.1257/aer.20180279.
38. Deryugina, T.; Heutel, G.; Miller, N.H.; Molitor, D.; Reif, J. The Mortality and Medical Costs of Air Pollution: Evidence from Changes in Wind Direction. *American Economic Review* **2019**, *109*, 4178–4219, doi:10.1257/aer.20180279.
39. Xie, Y.; He, Y.; Ye, Y.; Liu, C. Employ Mathematical Modeling to Summarize, Analyze, And Predict the Relationship Between Carbon Dioxide and Temperature, Location, And Other Factors. *Academic Journal of Science and Technology* **2024**, *11*, 13–20, doi:10.54097/y1jm6q63.
40. Liu, H.; Zhang, Z.; Cai, X.; Wang, D.; Liu, M. Investigating the Driving Factors of Carbon Emissions in China's Transportation Industry from a Structural Adjustment Perspective. *Atmos Pollut Res* **2024**, *15*, 102224, doi:10.1016/j.apr.2024.102224.
41. Liu, B.; Guan, Y.; Shan, Y.; Cui, C.; Hubacek, K. Emission Growth and Drivers in Mainland Southeast Asian Countries. *J Environ Manage* **2023**, *329*, 117034, doi:10.1016/j.jenvman.2022.117034.
42. Forkel, M.; Carvalhais, N.; Rödenbeck, C.; Keeling, R.; Heimann, M.; Thonicke, K.; Zaehle, S.; Reichstein, M. Enhanced Seasonal CO_2 Exchange Caused by Amplified Plant Productivity in Northern Ecosystems. *Science (1979)* **2016**, *351*, 696–699, doi:10.1126/science.aac4971.
43. Lin, X.; Rogers, B.M.; Sweeney, C.; Chevallier, F.; Arshinov, M.; Dlugokencky, E.; Machida, T.; Sasakawa, M.; Tans, P.; Keppel-Aleks, G. Siberian and Temperate Ecosystems Shape Northern Hemisphere Atmospheric CO_2 Seasonal Amplification. *Proceedings of the National Academy of Sciences* **2020**, *117*, 21079–21087, doi:10.1073/pnas.1914135117.
44. Le Quéré, C.; Jackson, R.B.; Jones, M.W.; Smith, A.J.P.; Abernethy, S.; Andrew, R.M.; De-Gol, A.J.; Willis, D.R.; Shan, Y.; Canadell, J.G.; et al. Temporary Reduction in Daily Global CO_2 Emissions during the COVID-19 Forced Confinement. *Nat Clim Chang* **2020**, *10*, 647–653, doi:10.1038/s41558-020-0797-x.
45. Chen, J.; Li, C.; Ristovski, Z.; Milic, A.; Gu, Y.; Islam, M.S.; Wang, S.; Hao, J.; Zhang, H.; He, C.; et al. A Review of Biomass Burning: Emissions and Impacts on Air Quality, Health and Climate in China. *Science of The Total Environment* **2017**, *579*, 1000–1034, doi:10.1016/j.scitotenv.2016.11.025.

46. Ji, X.; Long, X. A Review of the Ecological and Socioeconomic Effects of Biofuel and Energy Policy Recommendations. *Renewable and Sustainable Energy Reviews* **2016**, *61*, 41–52, doi:10.1016/j.rser.2016.03.026.
47. Field, R.D.; van der Werf, G.R.; Shen, S.S.P. Human Amplification of Drought-Induced Biomass Burning in Indonesia since 1960. *Nat Geosci* **2009**, *2*, 185–188, doi:10.1038/ngeo443.
48. Andreae, M.O.; Merlet, P. Emission of Trace Gases and Aerosols from Biomass Burning. *Global Biogeochem Cycles* **2001**, *15*, 955–966, doi:10.1029/2000GB001382.
49. Philip, S.; Johnson, M.S.; Potter, C.; Genovesse, V.; Baker, D.F.; Haynes, K.D.; Henze, D.K.; Liu, J.; Poulter, B. Prior Biosphere Model Impact on Global Terrestrial CO_2 Fluxes Estimated from OCO-2 Retrievals. *Atmos Chem Phys* **2019**, *19*, 13267–13287, doi:10.5194/acp-19-13267-2019.
50. Lee, D.S.; Fahey, D.W.; Skowron, A.; Allen, M.R.; Burkhardt, U.; Chen, Q.; Doherty, S.J.; Freeman, S.; Forster, P.M.; Fuglestvedt, J.; et al. The Contribution of Global Aviation to Anthropogenic Climate Forcing for 2000 to 2018. *Atmos Environ* **2021**, *244*, 117834, doi:10.1016/j.atmosenv.2020.117834.
51. Corbett, J.J.; Winebrake, J.J.; Green, E.H.; Kasibhatla, P.; Eyring, V.; Lauer, A. Mortality from Ship Emissions: A Global Assessment. *Environ Sci Technol* **2007**, *41*, 8512–8518, doi:10.1021/es071686z.
52. Landschützer, P.; Gruber, N.; Bakker, D.C.E.; Schuster, U. Recent Variability of the Global Ocean Carbon Sink. *Global Biogeochem Cycles* **2014**, *28*, 927–949, doi:10.1002/2014GB004853.
53. Takahashi, T.; Sutherland, S.C.; Wanninkhof, R.; Sweeney, C.; Feely, R.A.; Chipman, D.W.; Hales, B.; Friederich, G.; Chavez, F.; Sabine, C.; et al. Climatological Mean and Decadal Change in Surface Ocean PCO_2, and Net Sea–Air CO_2 Flux over the Global Oceans. *Deep Sea Research Part II: Topical Studies in Oceanography* **2009**, *56*, 554–577, doi:10.1016/j.dsr2.2008.12.009.
54. Bates, N.; Astor, Y.; Church, M.; Currie, K.; Dore, J.; Gonaález-Dávila, M.; Lorenzoni, L.; Muller-Karger, F.; Olafsson, J.; Santa-Casiano, M. A Time-Series View of Changing Ocean Chemistry Due to Ocean Uptake of Anthropogenic CO_2 and Ocean Acidification. *Oceanography* **2014**, *27*, 126–141, doi:10.5670/oceanog.2014.16.
55. Nassar, R.; Jones, D.B.A.; Suntharalingam, P.; Chen, J.M.; Andres, R.J.; Wecht, K.J.; Yantosca, R.M.; Kulawik, S.S.; Bowman, K.W.; Worden, J.R.; et al. Modeling Global Atmospheric CO_2 with Improved Emission Inventories and CO_2 Production from the Oxidation of Other Carbon Species. *Geosci Model Dev* **2010**, *3*, 689–716, doi:10.5194/gmd-3-689-2010.